International Journal of Thin Films Science and Technology

http://dx.doi.org/10.18576/ijtfst/150105

Photocatalytic Degradation of Cr(VI) via Electrospun MWCNTs-Fe_3O_4@PET and MWCNTs-Fe_3O_4/PET Nanofibers

Shahyan S. Ahmed[1], *Banaz A. Abdulghafar*[1], *Hadar M. Abdullah*[1], *Suhad A. Yasin*[1,*], *Rihan S. Abdul Jabar*[2,3], *Kwok Feng Chong*[4], *Gomaa A.M. Ali*[5], *and Zinab H. Bakr*[6]

[1] College of Science, University of Duhok, Duhok, 42001, Iraq
[2] Pharmacognosy, Faculty of Pharmacy, Cihan University- Duhok, Kurdistan Region, Iraq
[3] Department of Chemistry, College of Science, University of Zakho, Zakho, Kurdistan Region, Iraq
[4] Faculty of Industrial Sciences and Technology, Universiti Malaysia Pahang Al-Sultan Abdullah, Gambang, 26300, Kuantan, Pahang, Malaysia
[5] College of Marine Science and Aquatic Biology, University of Khorfakkan, 18119, Sharjah, United Arab Emirates
[6] Physics Department, Faculty of Science, Assiut University, Assiut 71516, Egypt

Received: 7 Nov. 2025, Revised: 7 Dec. 2025, Accepted: 19 Dec. 2025
Published online: 1 Jan. 2026

Abstract: Two approaches were used to synthesize and modify polyethylene terephthalate (PET) nanofibers for the photocatalytic reduction of Cr(VI) under xenon light. Fe_3O_4 nanoparticles were prepared via a simple hot water method and composited with PET nanofibers to form MWCNTs-Fe_3O_4@PET and electrospun MWCNTs-Fe_3O_4@PET nanofibers (NFs). XRD and SEM confirmed the smooth, homogeneous nanostructure. Photocatalytic activity was evaluated under various conditions (pH, contact time, Cr(VI) concentration, and reusability). MWCNTs-Fe_3O_4@PET NFs achieved 92% Cr(VI) reduction at pH 4 within 30 minutes, while MWCNTs-Fe_3O_4@PET reached 77.85% after 60 minutes. Reusability tests showed MWCNTs-Fe_3O_4@PET NFs retained 75% efficiency after four cycles. In contrast, MWCNTs-Fe_3O_4@PET NFs declined from 92.52% to 76.13% after one cycle due to its delicate texture. These findings suggest that while MWCNTs-Fe_3O_4@PET NFs offers higher initial efficiency, but, MWCNTs-Fe_3O_4@PET NFs provides better long-term reusability, making it a promising material for Cr(VI) removal from aqueous environments.

Keywords: Electrospinning, Chromium ions, Nanofiber, Multiwalled carbon nanotubes, Wastewater treatment and Sustainability.

1 Introduction

The rapid growth of industrialization and urbanization has led to water pollution, such as heavy metal contamination, that produces severe ecological problems that threaten environmental systems and human health [1,2,3,4]. Municipal solid waste largely consists of food and green waste (44%), paper (17%), and plastic (12%). However, plastics can take thousands of years to decompose, unlike organic waste, which can breakdown naturally [5,6,7]. Industrial activities, including tanning, electrochemical deposition, wood reservation, dye manufacturing, steel production, and chromate synthesis, can discharge hexavalent chromium (Cr(VI)) into the environment [8]. Cr(VI) is considered highly water soluble, highly hazardous, and carcinogenic to various organisms [9,10]. The maximum permitted levels of Cr(VI) discharge into surface water and drinking water are 0.1 ppm and 0.05 ppm, respectively, according to the World Health Organization (WHO) [11]. Industrial processes and wastewater treatment face notable problems such as a short lifetime, elevated production value, reusability, and recycling of homogeneous catalysts from the reaction mixture. Thus, Cr(VI) must be removed from water for the sake of the ecosystem. On the other hand, heterogeneous catalysts have recently been used as a substitute solution in water purification and decontamination because of their simplicity of handling, high catalytic capacity, simple collection, recyclability, minimal toxicity, and low cost [12,13]. The photocatalysts, hazardous metal ions, or metalloids used for the photocatalytic reduction of Cr(VI) have been

* Corresponding author e-mail: suhad.yasin@uod.ac

reduced to nontoxic matter that can be readily removed from aqueous solutions via additional processing [14,15, 16]. Moreover, the main advantage of this technology is the direct conversion of light into chemical energy, which decreases energy consumption as an environmentally friendly strategy to prevent environmental pollution [17, 18]. Among the numerous photocatalysts studied to remove Cr(VI) are the magnetic semiconductors of n-type metal oxide sustainable composites [19,20,21]. The biocompatible and large surface area effectively absorbs visible light with a low bandgap (1.4 eV) [22]. Today, the use of composite nanofibers for wastewater treatment by photocatalytic processes has attracted the attention of most researchers as a unique method because of their outstanding efficiency, economical cost [23] excellent electron conductivity [24], increased durability [25], ease of availability, chemical inertness, resistance to UV light and mechanical and environmental stability [17,23], Moreover, nanoparticles are also used as composites in general, and specifically, iron nanoparticles have received considerable scientific and technological interest. Numerous methods have been demonstrated for the synthesis of nanoparticles, and among these processes, a simple process has been applied that uses only hot water. Hot water treatment can produce nanoparticles of many metal oxides at low temperatures. The advantages of this technique include the low-cost equipment needed, environmentally friendly, highly productive, and catalyst-free [26]. The nanocomposites function as photocatalysts. When lit, these materials produce reactive species such as hydroxyl radicals and other reactive oxygen species, which are required for Cr(VI) reduction [27]. Additionally, the scientific community favours the use of the bulky specific surface area and membrane photocatalysts produced by the electrospinning technique, which can be reutilized through the electrospinning technique, through which various polymers can be used to create extremely porous nanofibrous structures [28,29, 30]. Integrating electrospinning technologies and photocatalysis can increase photocatalytic efficiency and reusability, reducing losses during recycling [31]. In addition, photocatalytic materials such as carbon nanotubes (CNTs) with large surface areas that have active sites on which photocatalytically active nanoparticles can be immobilized in an efficient manner can be utilized [32,33,34,35]. Multiwalled carbon nanotubes (MWCNTs) have superior physicochemical properties to increase the Young's modulus, chemical resistance, and tensile strength of the nanofibers. Additionally, CNTs have electron donor characteristics, resulting in increased photocatalytic activity [36]. Despite its greater ability to remove Cr(VI) ions, Fe_3O_4 is prone to forming agglomerates in aqueous solutions. To mitigate these detrimental effects, Fe_3O_4 can be combined with other components to create composites with improved stability, and composites such as Fe_3O_4@PSBC effectively remove Cr(VI) ions from wastewater [37]. Additionally, the literature has shown that strong photocatalytic performance was obtained for the photoreduction of Cr(VI), and the removal efficiency was improved under lower pH conditions [38]. This study involved the modification of PET nanofibers with a nanocomposite (MWCNTs-Fe_3O_4) via two techniques, namely, immersion and electrospinning, and compared their properties and ability to remove Cr(VI) from water. In the first composite, MWCNTs-Fe_3O_4@PET NFs, PET was fabricated via an electrospinning technique, followed by additional crosslinking of the surface-modified MWCNTs-Fe_3O_4 onto the electrospun PET, enhances heavy-metal adsorption by introducing many active binding sites on the surface of the material (MWCNTs-Fe_3O_4). In the second composite, MWCNTs-Fe_3O_4/PET, a blended mixture of prepared Fe_3O_4, MWCNTs, and PET solution, was fabricated via an electrospinning technique. The MWCNTs-Fe_3O_4/PET composite prepared via the electroplating technique has a high surface area and shows greater stability after reuse. The crosslinked composite also yields greater chromium crushing efficiency from water. Furthermore, the degradation process was investigated kinetically by studying the influence of pH, contact time, and Cr(VI) dose on both composites. Thus, this approach provides a prospective way to prepare heterogeneous nanocatalysts for extensive applications in the degradation and reduction of micropollutants. More importantly, photocatalysts have powerful recoverability and are simple to separate and recycle with the use of an external magnet.

2 Experimental procedures

2.1 Materials

Polyethylene terephthalate (PET) polymers are supplied from waste sources. Dichloromethane (DCM) and acetone were purchased from Scharlau, and Ricca Chemical Company supplied sulfuric acid and hydrochloric acid. Sodium hydroxide was obtained from Sigma–Aldrich, potassium dichromate ($K_2Cr_2O_7$) was used to obtain different Cr(VI) concentrations, and iron (Fe) powder was obtained from BDH Chemicals Ltd. (Poole England). 1,5-Diphenylcarbazide (DPC) and trifluoroacetic acid (TFA) were obtained from ROTH Chemical Company, and glutaraldehyde (GA) was obtained from Raedel-de Haen Ag Sleeze Hannover. (MWCNTs) from the National and Medical Science Research Center, Nizwa, Oman.

2.2 Synthesis of Fe_3O_4 Nanoparticles

First, the Fe powder was purified from impurities, cleaned with deionized water and acetone, and then dried in a closed container to avoid corrosion. Second, 1 g of

cleaned iron powder was mixed with 20 ml of deionized water and heated to 75 °C for 1.5 h with stirring. These conditions were defined to be the best and critical for the complete formation of iron oxide nanoparticles [26,39]. Finally, the nanoparticles were separated and dried in an oven until analysis.

2.3 Synthesis of MWCNTs-Fe_3O_4/PET NFs

First, the PET polymer solution was prepared by mixing DCM and TFA (3:1) with the PET solution, and the mixture was stirred continuously for 4 h at room temperature. The prepared solution was subsequently mixed with 1% MWCNTs (provided by the National and Medical Science Research Center, Nizwa, Oman) and magnetite NPs at a ratio of 1:1. Next, the blended mixture was electrospun by transforming it into a syringe joined with a needle of stainless steel. The operators of the electrospinning device were as follows: 5% PET solution, 15 cm distance between the tip of the needle and the collector, 15 kV operating voltage, and 1 ml/h flow rate [40].

2.4 Preparation of MWCNTs-Fe_3O_4@PET NFs

For the preparation of the MWCNTs-Fe_3O_4 on the surface of the PET nanofibers, the PET polymer solution was prepared in the same way as previously mentioned and electrospun under similar conditions. A 100 mL solution containing deionized water with 2.5% GA was used as a crosslinking agent to immerse the PET nanofibers for 24 h. After that, the crosslinking agent was separated, washed, and dried. Five percent MWCNTs and 1% Fe_3O_4 NPs (5:1) were prepared, and approximately 10 ml of the obtained MWCNT and Fe_3O_4 NP mixture was poured onto the nanofibers and left for 24 h. Finally, the modified nanofibers were rinsed with deionized water and ethanol, then air-dried for use in subsequent experiments.

2.5 Characterization

The resulting composite nanofiber membranes were morphologically studied via SEM (JEOL SEM7000FE). The XRD pattern was recorded with a Bruker D8-Discover diffractometer, and to determine the levels of Cr(VI) in aqueous solutions, a UV–Vis Jenway-7315 spectrophotometer was used.

2.6 Photocatalytic assessments

Photocatalytic tests were carried out to determine the effects of pH (2–10), contact time and initial Cr(VI) concentration under a xenon lamp (125 W) on the photoreduction of Cr(VI) by the composite nanofiber membrane. These experiments were performed in conical flasks, with 10 ml of Cr(VI) ranging from 20 to 100 mg L-1 and 0.005 gm of nanofiber composite. For adsorption equilibration of Cr(VI), the synthesized composites were placed into conical flasks and mixed with Cr(VI) solution at room temperature in darkness for 30 min. After equilibration, the solutions were irradiated with xenon light, and the distance between the source of light and the membranes was 15 cm. For the analysis at each interval, 3 ml of the suspension was removed. The concentration of Cr(VI) in the solutions was examined via a UV-visible spectrophotometer at 541 nm after complexation with diphenylcarbazide and dilution with H_2SO_4 [41]. The photocatalytic performance of Cr(VI) is as follows:

Photocatalytic Efficiency (%) $=C_o\text{-}C_f/C_o\times100$

where C_o and C_f are the initial and final Cr(VI) concentrations (mg/l), respectively. The reaction rate of the Cr(VI) photodegradation experiment was calculated via pseudo-first-order kinetics:

$Ln(C_oC_t)=k_t$ where C_o is the initial concentration of Cr(VI), C_t is the measured concentration of Cr(VI) degradation at different irradiation times, and k_t is the reaction rate of Cr(VI) degradation.

3 Results and Discussion

3.1 Characterization of the MWCNT-Fe_3O_4@PET NFs and MWCNTs-Fe_3O_4/PET NFs nanofiber composites

Figure 1 shows the MWCNTs-Fe_3O_4@PET NFs and MWCNTs-Fe_3O_4/PET NFs composites before and after photodegradation. The successful fabrication of MWCNTs-Fe_3O_4 on the surface of Figure 1(a, b) shows the successful deposition of MWCNTs-Fe_3O_4 on the surface of the PET nanofibers before and after photodegradation. The nanoparticles were still well-agglomerated and strongly crosslinked to the nanofiber even after Cr(VI) photodegradation, as depicted in Figure 1b. Figure 1c shows the incorporation of MWCNTs and Fe_3O_4 nanoparticles within the PET nanofibers. Nanoparticles can also be observed inside the fibers, which is ascribed to the electrically conductive nature of MWCNTs, as it enhances the conductivity of the solution and therefore forms nanofibers with smaller diameters, as can be seen in Figure 1d.

The XRD patterns of the MWCNTs-Fe_3O_4@PET and MWCNTs-Fe_3O_4/PET NFs shown in Figure 2 (patterns a, c) correspond to the diffraction peaks of the magnetite orthorhombic phase Fe_3O_4 (JCPDS Ref. Cod 98-026-5010) and the graphite sheets of the MWCNTs (JCPDS Ref. Cod 98-008-8812), PET, respectively. Typical (002) and (100) planes of the MWCNTs are

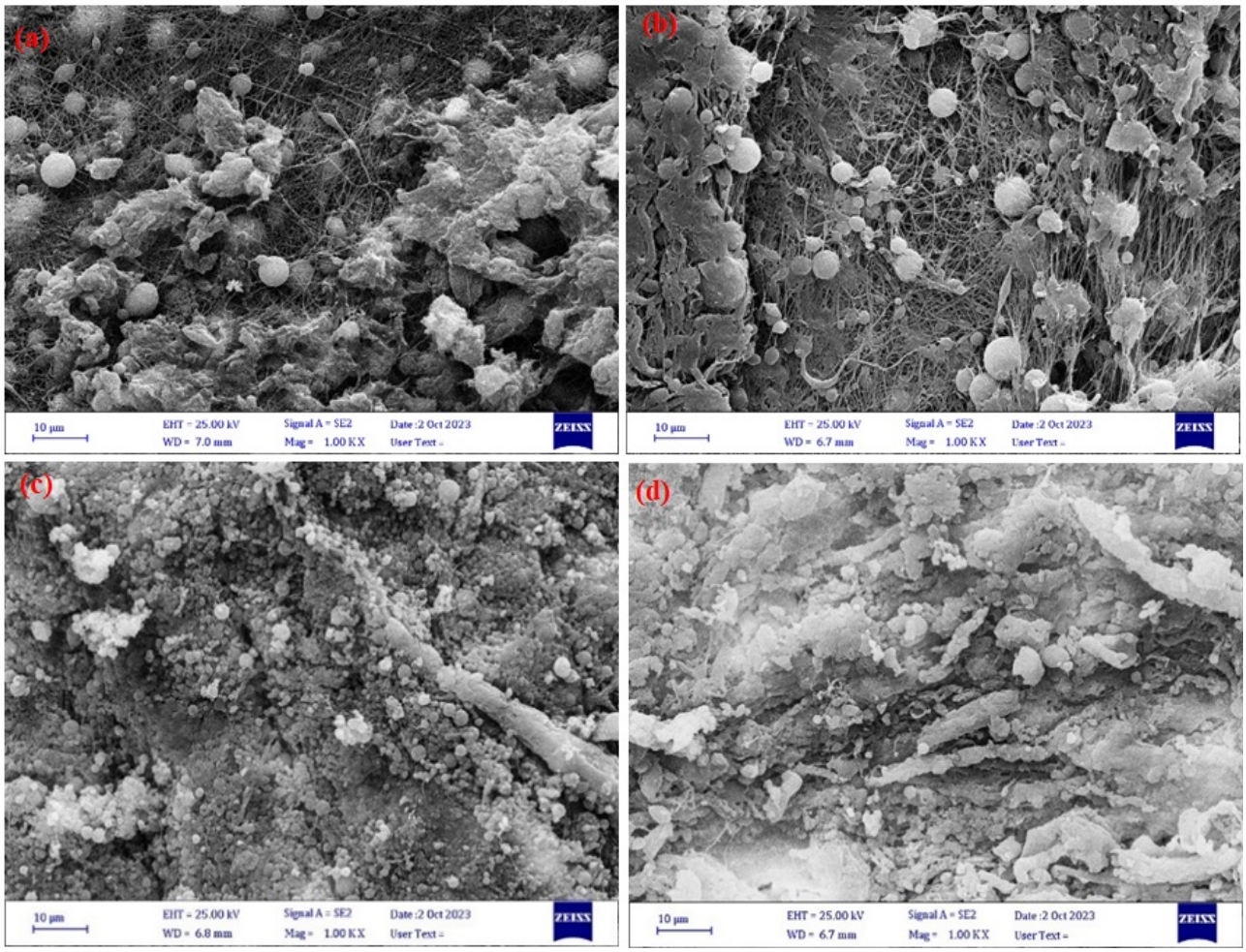

Fig. 1: SEM images of (a, b) MWCNTs-Fe_3O_4@PET NFs before and after photodegradation and (c, d) MWCNTs-Fe_3O_4/PET NFs before and after photodegradation.

observed at 20 values of 26.3° and 43°, respectively, which is consistent with previous results [42], whereas the peak at 21° related to the PET nanofiber and the peaks at 30.3°, 35.8°, 53.8°, and 56.8° are assigned to (220), (311), (511), and (440), respectively, and can be easily indexed to the Fe_3O_4 NPs. Thus, the XRD patterns confirmed the crystallinity of the synthesized MWCNTs-Fe_3O_4/PET NFs and MWCNTs-Fe_3O_4@PET NFs. In addition, the presence of the same diffraction peaks after photodegradation (patterns b and d) demonstrates the stability of the composite nanofibers [19].

3.2 Photocatalytic Performance

Some experiments were performed with various irradiation times, pH values, and concentrations of Cr(VI) for the MWCNTs-Fe_3O_4@PET NFs and MWCNTs-Fe_3O_4/PET NFs composite membranes. The results obtained by varying these parameters are presented in Figure 3. The Cr(VI) concentration was investigated via a UV–Visible spectrophotometer at 541 nm. The following is a discussion of the various parameters and their effects on dye degradation.

3.2.1 Effect of irradiation time

The calculated efficiencies of the photodegradation of Cr(VI) as a function of the irradiation time for the MWCNTs-Fe_3O_4/PET and MWCNTs-Fe_3O_4@PET NFs composite membranes are presented in Figure 3a. All the experiments were conducted at 20 mg/l Cr(VI) and pH 4. The photocatalytic efficiency of Cr(VI) increased for the MWCNTs-Fe_3O_4/PET NFs composites with increasing irradiation time up to 30 min (92%), whereas from 30-120 min of irradiation, the Cr(VI) degradation efficiency increased slowly because most of the catalyst

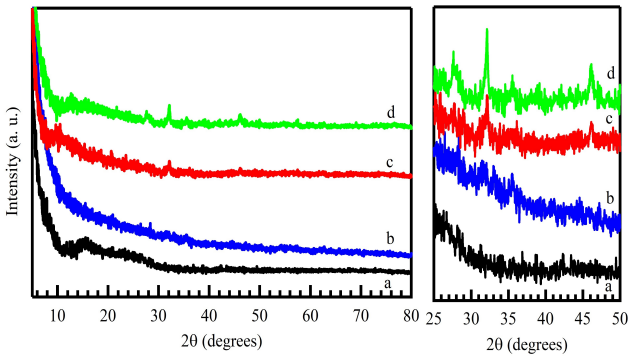

Fig. 2: XRD patterns of MWCNTs-Fe_3O_4/PET NFs and MWCNTs-Fe_3O_4@PET NFs before and after photodegradation. (a, b) MWCNTs-Fe_3O_4/PET NFs before and after photodegradation, respectively (c, d) MWCNTs-Fe_3O_4@PET NFs before and after photodegradation, respectively.

active surfaces were occupied, and the Cr(VI) particles present in the solution were mineralized. The photocatalytic efficiency of MWCNTs-Fe_3O_4@PET NFs increased gradually and reached a maximum value of 77.85% at 60 min, after which all the active sites of the photocatalysts were blocked, and the process reached equilibrium [43]. The results revealed that the maximum photocatalytic efficiency of Cr(VI), 92%, occurred at 30 min when the MWCNTs-Fe_3O_4/PET NFs were used, whereas for the MWCNTs-Fe_3O_4@PET NFs, only 67% photodegradation efficiency was observed under the same conditions. Such results are attributed to the larger surface area surface area and more active sites for the electrospun Fe_3O_4/PET NFs compared to the crosslinked composite Fe_3O_4@PET NFs.

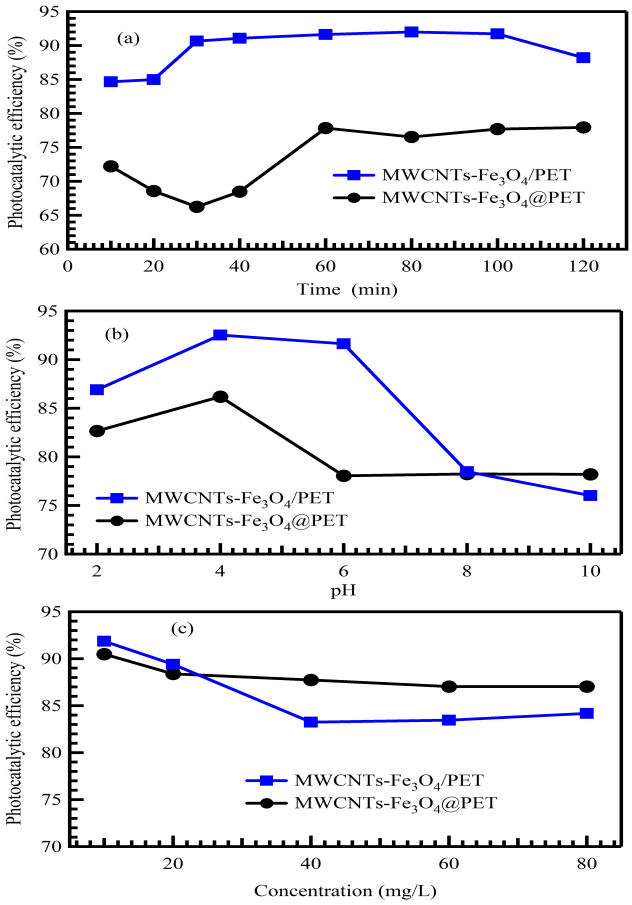

Fig. 3: The effects of irradiation time at pH= 4 (a), pH (b), and concentration (c) on the photocatalytic efficiency of the MWCNTs-Fe_3O_4/PET NFs and MWCNTs-Fe_3O_4@PET NFs membranes.

3.2.2 Effect of pH

The pH of a solution has a significant role in the photodegradation process because of its influence on the surface charge of the photocatalyst, interfacial electron transfer, and speciation of the metal ions in the solution [44]. The influence of pH on the photocatalytic performance of Cr(VI) by the MWCNTs-Fe_3O_4@PET NFs and MWCNTs-Fe_3O_4/PET NFs membranes was determined by using different pH solutions ranging from 2–10 at 20 mg/l Cr(VI) and 90 min of radiation, and 0.1 M NaOH and 0.1 M HCl were used to adjust the pH values, as shown in Figure 3b. The results demonstrated that the highest photoreduction was achieved in an acidic medium at pH 4 for both composites, with 92% for the MWCNTs-Fe_3O_4/PET NFs and 86% for the MWCNTs-Fe_3O_4@PET NFs, whereas it decreased to 76% at pH 8 for both composites. This can be explained by the electrostatic interactions between the positively charged iron oxide and the negatively charged ions of Cr(VI), which exist as oxyanions (CrO_4^{-2}, $Cr_2O_7^{-2}$, or $HCrO_4^{-}$) in acidic media [45]. In the basic medium, owing to the electrostatic repulsion between the photocatalyst, which has a more negative charge, and the dichromate ions, the photocatalytic efficiency of Cr(VI) decreases. The photocatalytic process is highly influenced by the pH of the solution, as it influences the surface charge of the semiconductor; as a result, it affects the adsorption, interfacial electron transfer, and photoreduction processes in addition to the speciation of the metal ions in the solution [41]. For the photoreduction of Cr(VI) to proceed, the conduction band of the catalyst must be more negative than the Cr(VI) potential reduction. In basic media, the potential reduction of Cr(VI) is more negative than that of photogenerated electrons; as a result, an acidic medium is needed. Moreover, higher pH values shift the position of the

valence band and conduction band to a higher cathodic potential by 59 mV per pH unit[46].

3.2.3 Effect of the Cr(VI) concentration

To illustrate the impact of the Cr(VI) concentration on the photocatalytic ability of both composites, as shown in Figure 3c, different concentrations (from 10 to 80 mg/l) of Cr(VI) were used at pH 4 for 90 min as the irradiation time. The highest reduction, 92%, was achieved at a 10 mg/l Cr(VI) concentration. However, the photocatalytic efficiency of Cr(VI) decreased from 92% to 85% when the Cr(VI) concentration increased from 10–80 mg/l, and it still exhibited high efficiency at high concentrations, confirming the potential effectiveness of these composites in Cr(VI) degradation. The higher the Cr(VI) level is, the lower the composite efficiency for Cr(VI) photocatalysis. This can be attributed to the fact that increasing Cr(VI) concentration causes more light to be absorbed before it reaches the catalyst surface, thereby reducing the extent of reduction. Furthermore, an increase in the Cr(VI) concentration may cause the active sites on the catalyst surface to become saturated, leading to a decrease in the photoreduction efficiency. Finally, high levels of Cr(VI) may lead to the overloading of photocatalyst active sites and their deactivation, resulting in decreased photocatalytic reduction of Cr(VI) [47,48].

3.2.4 Performance in the Photocatalytic Reduction of Cr(VI)

In terms of degradation efficiency, the data in Figure 4 show the performance in the photocatalytic reduction of Cr(VI) using two different catalysts: MWCNTs-Fe_3O_4@PET NFs and MWCNTs-Fe_3O_4/PET NFs. The initial concentration was greater for the MWCNTs-Fe_3O_4@PET NFs than for the MWCNTs-Fe_3O_4/PET NFs. Compared with the MWCNTs-Fe_3O_4/PET NFs, the MWCNTs-Fe_3O_4@PET NFs fluctuate more in concentration, indicating a less stable reduction process. The MWCNTs-Fe_3O_4/PET NFs exhibited a more stable and continuous reduction in the Cr(VI) concentration over the observed period. By the end of 120 min, the MWCNTs-Fe_3O_4/PET NFs achieved a significantly lower concentration of Cr(VI) than did the PET@MWCNTs-Fe_3O_4 NFs, indicating better overall performance in reducing Cr(VI). In conclusion, the MWCNTs-Fe_3O_4/PET NFs catalyst demonstrated a more effective and consistent reduction of Cr(VI) over the 120-minute period, achieving a lower final concentration than the MWCNTs-Fe_3O_4@PET NFs. Moreover, the kinetic linear curve of the MWCNTs-Fe_3O_4@PET NFs during Cr(VI) photodegradation showed that the degradation followed a simplified Langmuir first-order model, as indicated by R^2= 0.81 with a rate constant equal to 0.004 min^{-1}, confirming the pseudo first-order reaction.

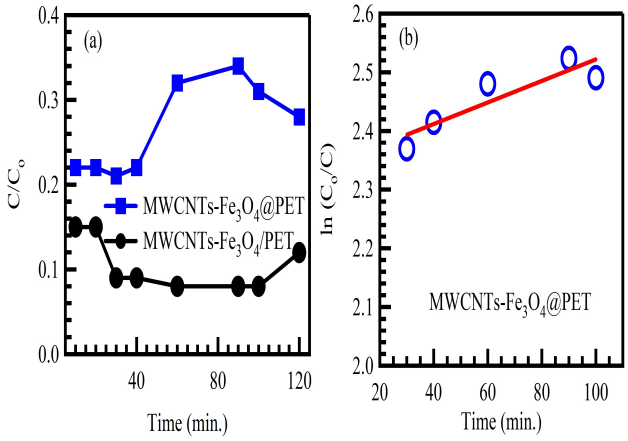

Fig. 4: (a) Effect of contact time on the photodegradation of Cr(VI) by MWCNTs-Fe_3O_4@PET and MWCNTs-Fe_3O_4/PET NFs and (b) fitting of the pseudo-first-order of MWCNTs-Fe_3O_4/PET NFs.

3.2.5 Regeneration and reusability of photocatalysis

To assess the reusability and cost-effectiveness of the composites for the photocatalytic reduction of Cr(VI), regeneration and reuse are crucial factors. The durability of both composites was determined at pH 4, 20 mg/l, and 90 min, as shown in Figure 5. After each cycle, the two composites were collected and washed with HCl and deionized water, dried, and subjected to the same reaction conditions. The results show that the MWCNTs-Fe_3O_4@PET NFs composite retained its efficiency after 4 cycles. The photocatalytic efficiency of the MWCNTs-Fe_3O_4@PET NFs decreased at cycle 5, which could be due to the surface of the catalysts being deactivated after consecutive cycles [49]. Moreover, the membrane efficiency of the electrospun composite MWCNTs-Fe_3O_4/PET NFs composite nanofiber was reduced after the first cycle, which might have been caused by composite loss through the washing process [50] due to its delicate texture/form, as shown in Figure 5.

4 Conclusion

To conclude, the goal of this study was to prepare MWCNTs-Fe_3O_4/PET NFs and MWCNTs-Fe_3O_4@PET NFs composite nanofiber membranes via economic and efficient methods and to use the composites for the photodegradation of Cr(VI) in wastewater via xenon light. The electrospinning method was successfully used for the preparation of the two composites, and the NPs were mixed with the PET solution and ladened to the nanofiber surface to obtain composite nanofibers. The photodegradation was pH dependent, and the efficiency

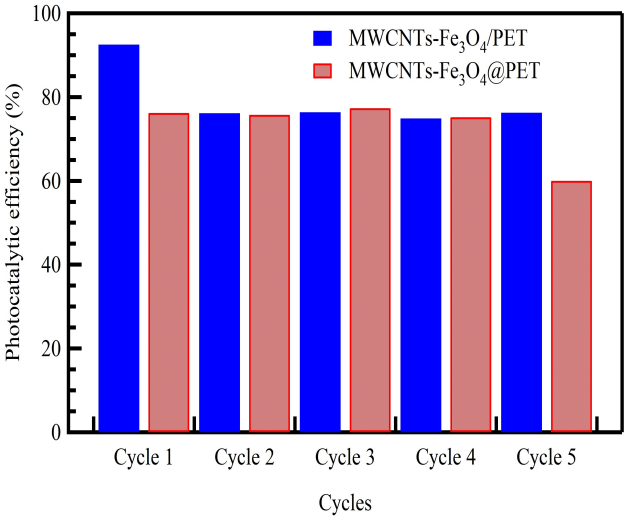

Fig. 5: Reusability of the composite nanofibers for the photodegradation of Cr(VI) after 5 cycles for the MWCNTs-Fe_3O_4@PET NFs and MWCNTs-Fe_3O_4/PET NFs composite nanofiber membranes.

was highest at an acidic pH of 4 (92%) for the MWCNTs-Fe_3O_4 NPs/PET NFs and 86% for the MWCNTs-Fe_3O_4@PET NFs, whereas it reached 78% at pH 8 for both composites. The photocatalytic efficiency of the MWCNTs-Fe_3O_4/PET NFs was faster than that of the MWCNTs-Fe_3O_4@PET NFs, and the maximum photodegradation efficiency of Cr(VI) was 92% after 30 min. In addition, the photocatalytic efficiency of Cr(VI) decreased from 92 to 83% for the MWCNTs-Fe_3O_4/PET NFs but decreased from 90.5% to 88% for the MWCNTs-Fe_3O_4@PET NFs when the concentration increased from 10–40 mg/l. Furthermore, after four cycles of Cr(VI) photodegradation, the Fe_3O_4 @PET NFs maintained high performance, stability, and reusability, achieving an efficiency of approximately 75%, whereas the MWCNTs-Fe_3O_4/PET NFs decreased after the first cycle and remained stable for other cycles. The results of this study showed that the catalyst materials have potential for effective and economic photodegradation of Cr(VI) from many industrial wastewaters.

References

[1] Guo, D.-M.; An, Q.-D.; Xiao, Z.-Y.; Zhai, S.-R.; Shi, Z.; Polyethylenimine-functionalized cellulose aerogel beads for efficient dynamic removal of chromium(vi) from aqueous solution. RSC Advances 2017, 7,54039-54052.

[2] Gadore, V.; Singh, A. K.; Mishra, S. R.; Ahmaruzzaman, M.; RSM approach for process optimization of the photodegradation of congo red by a novel $NiCo_2S_4$/chitosan photocatalyst. Scientific Reports 2024, 14.

[3] Shayegan, H.; Ali, G. A. M.; Safarifard, V.; Recent Progress in the Removal of Heavy Metal Ions from Water Using Metal-Organic Frameworks. ChemistrySelect 2020, 5, 124-146.

[4] Adil, H. I.; Thalji, M. R.; Yasin, S. A.; Saeed, I. A.; Assiri, M. A.; Chong, K. F.; Ali, G. A. M.; Metal–organic frameworks (MOFs) based nanofiber architectures for the removal of heavy metal ions. RSC Advances 2022, 12, 1433-1450.

[5] Xiao, Y.; Tian, Y.; Xu, W.; Zhu, J. in Photodegradation of microplastics through nanomaterials: Insights into photocatalysts modification and detailed mechanisms, Vol. MDPI AG, 2024.

[6] Zahrah, Y.; Yu, J.; Liu, X.; How Indonesia's Cities Are Grappling with Plastic Waste: An Integrated Approach towards Sustainable Plastic Waste Management. Sustainability 2024, 16, 3921.

[7] Alhanish, A.; Ali, G. A. M. in Recycling the Plastic Wastes to Carbon Nanotubes, Vol. Springer International Publishing, 2021, pp. 701-727.

[8] Zhong, Y.; Qiu, X.; Chen, D.; Li, N.; Xu, Q.; Li, H.; He, J.; Lu, J.; Flexible Electrospun Carbon Nanofiber/Tin(IV) Sulfide Core/Sheath Membranes for Photocatalytically Treating Chromium(VI)-Containing Wastewater. ACS Applied Materials and Interfaces 2016, 8, 28671-28677.

[9] Zhang, C.; Li, X.; Bian, X.; Zheng, T.; Wang, C.; Polyacrylonitrile/manganese acetate composite nanofibers and their catalysis performance on chromium (VI) reduction by oxalic acid. Journal of Hazardous Materials 2012, 229-230, 439-445.

[10] Majigsuren, E.; Byambasuren, U.; Bat-Amgalan, M.; Mendsaikhan, E.; Kano, N.; Kim, H. J.; Yunden, G.; Adsorption of Chromium (III) and Chromium (VI) Ions from Aqueous Solution Using Chitosan–Clay Composite Materials. Polymers 2024, 16, 1399.

[11] Golabiazar, R.; Sabr, M. R.; Ali, A. A.; Qadr, N. S.; Rahman, R. S.; Othman, K. I.; Khalid, K. M.; Musa, S. J.; Hamadammin, B. J.; Investigation and characterization of biosynthesized green adsorbent CuO NPs and CuO/Fe_3O_4 NCs using Adiantum C.V leaf for removal MO dye and Cr(VI) metal ions: thermodynamic, kinetic, and antibacterial studies. Journal of the Iranian Chemical Society 2022, 19, 3135-3153.

[12] Chowdhury, A.; Khan, A. A.; Kumari, S.; Hussain, S.; Superadsorbent Ni–Co–S/SDS Nanocomposites for Ultrahigh Removal of Cationic, Anionic Organic Dyes and Toxic Metal Ions: Kinetics, Isotherm and Adsorption Mechanism. ACS Sustainable Chemistry Engineering 2019, 7, 4165-4176.

[13] Pérez-Lucas, G.; Campillo, A.; Navarro, S.; Impact of Inorganic Anions on the Photodegradation of Herbicide Residues in Water by UV/Persulfate-Based Advanced Oxidation. Catalysts 2024, 14, 376.

[14] Ajiboye, T. O.; Oyewo, O. A.; Onwudiwe, D. C.; Conventional and Current Methods of Toxic Metals Removal from Water Using g-C_3N_4-Based Materials. Journal of Inorganic and Organometallic Polymers and Materials 2020, 31, 1419-1442.

[15] Litter, M. I.; Mechanisms of removal of heavy metals and arsenic from water by TiO_2-heterogeneous photocatalysis. Pure and Applied Chemistry 2015, 87, 557-567.

[16] Govinda, V.; A, S. R.; Prasad, C.; Sambasivam, S.; Bahadur, I.; Katata-Seru, L. M.; Mohammad, F.; Abedigamba, O.

P.; Choi, H. Y.; Congo red dye reduction mediated by the electron (e) transfer route of BH_4 ions using synthesized $NiCo_2O_4$/rGO hybrid nanosheets. Materials Research Express 2024, 11, 065003.

[17] Melinte, V.; Stroea, L.; Chibac-Scutaru, A. L.; Polymer Nanocomposites for Photocatalytic Applications. Catalysts 2019, 9, 986.

[18] Dehghani, M. T.; Delnavaz, M.; UV-light-responsive Ag/TiO_2/PVA nanocomposite for photocatalytic degradation of Cr, Ni, Zn, and Cu heavy metal ions. Scientific Reports 2024, 14.

[19] Mohamed, A.; Yousef, S.; Ali, S.; Sriubas, M.; Varnagiris, S.; Tuckute, S.; Abdelnaby, M. A.; Kamel, B. M.; Highly Efficient Visible Light Photodegradation of Cr(VI) Using Electrospun MWCNTs-Fe_3O_4@PES Nanofibers. Catalysts 2021, 11, 868.

[20] Sibhatu, A. K.; Weldegebrieal, G. K.; Sagadevan, S.; Tran, N. N.; Hessel, V.; Photocatalytic activity of CuO nanoparticles for organic and inorganic pollutants removal in wastewater remediation. Chemosphere 2022, 300, 134623.

[21] Sadegh, H.; Ali, G. A. M.; Makhlouf, A. S. H.; Chong, K. F.; Alharbi, N. S.; Agarwal, S.; Gupta, V. K.; MWCNTs-Fe_3O_4 nanocomposite for Hg(II) high adsorption efficiency. Journal of Molecular Liquids 2018, 258, 345-353.

[22] Ge, T.; Jiang, Z.; Shen, L.; Li, J.; Lu, Z.; Zhang, Y.; Wang, F.; Synthesis and application of Fe_3O_4/$FeWO_4$ composite as an efficient and magnetically recoverable visible light-driven photocatalyst for the reduction of Cr(VI). Separation and Purification Technology 2021, 263, 118401.

[23] Salama, A.; Mohamed, A.; Aboamera, N. M.; Osman, T. A.; Khattab, A.; Photocatalytic degradation of organic dyes using composite nanofibers under UV irradiation. Applied Nanoscience 2018, 8, 155-161.

[24] Ajiboye, T. O.; Oyewo, O. A.; Marzouki, R.; Onwudiwe, D. C.; Photocatalytic Reduction of Hexavalent Chromium Using Cu3.21Bi4.79S9/g-C_3N_4 Nanocomposite. Catalysts 2022, 12, 1075.

[25] Ateia, M.; Alalm, M. G.; Awfa, D.; Johnson, M. S.; Yoshimura, C.; Modeling the degradation and disinfection of water pollutants by photocatalysts and composites: A critical review. Science of The Total Environment 2020, 698, 134197.

[26] Abdulghafar, B. A.; Yasin, S. A.; Saadi, N. S.; Modification of PVA Nanofiber by Simple Hot Water Treatment and Application on the Removal of Malachite Green Dye From Aqueous Solutions. Acta Chimica Slovenica 2024, 71, 398-408.

[27] Stegarescu, A.; Cabrera, H.; Budasheva, H.; Soran, M.-L.; Lung, I.; Limosani, F.; Korte, D.; Amati, M.; Borodi, G.; Kacso, I.; Opriş, O.; Dan, M.; Bellucci, S.; Synthesis and Characterization of MWCNT-COOH/Fe_3O_4 and CNT-COOH/Fe_3O_4/NiO Nanocomposites: Assessment of Adsorption and Photocatalytic Performance. Nanomaterials 2022, 12, 3008.

[28] Lv, H.; Liu, Y.; Bai, Y.; Shi, H.; Zhou, W.; Chen, Y.; Liu, Y.; Yu, D.-G.; Recent Combinations of Electrospinning with Photocatalytic Technology for Treating Polluted Water. Catalysts 2023, 13, 758.

[29] Ahmed, F. E.; Lalia, B. S.; Hashaikeh, R.; A review on electrospinning for membrane fabrication: Challenges and applications. Desalination 2015, 356, 15-30.

[30] Yasin, S.; Bakr, Z. H.; Ali, G. A. M.; Saeed, I. in Recycling Nanofibers from Polyethylene Terephthalate Waste Using Electrospinning Technique, Vol. Springer International Publishing, 2021, pp. 805-821.

[31] Cao, X.; Chen, W.; Zhao, P.; Yang, Y.; Yu, D.-G.; Electrospun Porous Nanofibers: Pore-Forming Mechanisms and Applications for Photocatalytic Degradation of Organic Pollutants in Wastewater. Polymers 2022, 14, 3990.

[32] Friehs, E.; AlSalka, Y.; Jonczyk, R.; Lavrentieva, A.; Jochums, A.; Walter, J.-G.; Stahl, F.; Scheper, T.; Bahnemann, D.; Toxicity, phototoxicity and biocidal activity of nanoparticles employed in photocatalysis. Journal of Photochemistry and Photobiology C: Photochemistry Reviews 2016, 29, 1-28.

[33] Ibrahim, A. S.; Farage, D. A. M.; Ali, G. A. M. in Biodegradation of Carbon Nanotubes, Vol. Springer International Publishing, 2022, pp. 1-34.

[34] Sadegh, H.; Ali, G. A. M.; Dodangeh, F.; Nadagouda, M. N.; Adsorption of Ammonium Ions onto Multi-Walled Carbon Nanotubes. Studia Universitatis Babeș-Bolyai Chemia 2017, 62, 233-245.

[35] Seyed Arabi, S. M.; Lalehloo, R. S.; Olyai, M. R. T. B.; Ali, G. A. M.; Sadegh, H.; Removal of congo red azo dye from aqueous solution by ZnO nanoparticles loaded on multiwall carbon nanotubes. Physica E: Low-dimensional Systems and Nanostructures 2019, 106, 150-155.

[36] Mohamed, A.; Nasser, W. S.; Kamel, B. M.; Hashem, T.; Photodegradation of phenol using composite nanofibers under visible light irradiation. European Polymer Journal 2019, 113, 192-196.

[37] Yu, C.; Liao, Y.; Removal of Cr(VI) ions from wastewater by Fe_3O_4-loaded porous sludge biochar. Water Science and Technology 2023, 88, 947-960.

[38] Ke, T.; Guo, H.; Zhang, Y.; Liu, Y.; Photoreduction of Cr(VI) in water using $BiVO_4$-Fe_3O_4 nano-photocatalyst under visible light irradiation. Environmental Science and Pollution Research 2017, 24, 28239-28247.

[39] Saadi, N. S.; Hassan, L. B.; Karabacak, T.; Metal oxide nanostructures by a simple hot water treatment. Scientific Reports 2017, 7.

[40] Yasin, S. A.; Sharaf Zeebaree, S. Y.; Sharaf Zeebaree, A. Y.; Haji Zebari, O. I.; Saeed, I. A.; The Efficient Removal of Methylene Blue Dye Using CuO/PET Nanocomposite in Aqueous Solutions. Catalysts 2021, 11, 241.

[41] Abdullah, H. M.; Ahmed, S. S.; Abdulghafar, B. A.; Yasin, S. A.; Zeebaree, S. Y. S.; Zeebaree, A. Y. S.; Zebari, O. I. H.; Enhanced water treatment with TEMPO-modified luffa cellulose-PVA nanofiber composite for removal of hexavalent chromium. Results in Chemistry 2024, 8, 101582.

[42] Nulu, A.; Nulu, V.; Sohn, K. Y.; Silicon and porous MWCNT composite as high capacity anode for lithium-ion batteries. Korean Journal of Chemical Engineering 2020, 37, 1795-1802.

[43] Ashar, A.; Bhatti, I. A.; Jilani, A.; Mohsin, M.; Rasul, S.; Iqbal, J.; Shakoor, M. B.; Al-Sehemi, A. G.; Wageh, S.; Al-Ghamdi, A. A.; Enhanced Solar Photocatalytic Reduction of Cr(VI) Using a (ZnO/CuO) Nanocomposite Grafted onto a Polyester Membrane for Wastewater Treatment. Polymers 2021, 13, 4047.

[44] Mohamed, A.; Osman, T. A.; Toprak, M. S.; Muhammed, M.; Yilmaz, E.; Uheida, A.; Visible light photocatalytic

reduction of Cr(VI) by surface modified CNT/titanium dioxide composites nanofibers. Journal of Molecular Catalysis A: Chemical 2016, 424, 45-53.

[45] Szabó, M.; Kalmár, J.; Ditrói, T.; Bellér, G.; Lente, G.; Simic, N.; Fábián, I.; Equilibria and kinetics of chromium(VI) speciation in aqueous solution – A comprehensive study from pH 2 to 11. Inorganica Chimica Acta 2018, 472, 295-301.

[46] Zhao, Z.; An, H.; Lin, J.; Feng, M.; Murugadoss, V.; Ding, T.; Liu, H.; Shao, Q.; Mai, X.; Wang, N.; Gu, H.; Angaiah, S.; Guo, Z.; Progress on the Photocatalytic Reduction Removal of Chromium Contamination. The Chemical Record 2018, 19, 873-882.

[47] Alelyani, S. S.; Kavil, Y. N.; Al-Farawati, R. K.; Zobidi, M.; Salam, M. A.; Shaban, Y. A.; Superior photocatalytic aptitude of MWCNT/TiO_2 for the removal of Cr (VI) from polluted water. Research on Chemical Intermediates 2023, 49, 1819-1842.

[48] Shaban, Y. A.; Effective Photocatalytic Reduction of Cr(VI) by Carbon Modified (CM)-n-TiO_2 Nanoparticles under Solar Irradiation. World Journal of Nano Science and Engineering 2013, 03, 154-160.

[49] Mavinakere Ramesh, A.; Shivanna, S.; Visible Light Assisted Photocatalytic Degradation of Chromium (VI) by Using Nanoporous Fe_2O_3. Journal of Materials 2018, 2018, 1-13.

[50] Solanki, R.; Jarosova, M.; Al-Azzawi, W. K.; Machek, P.; Alsultany, F. H.; Khalaji, A. D.; Al Mashhadani, Z. I.; Sonochemical-assisted synthesis of Fe_2O_3 nanoparticles and their photocatalytic activity toward methylene blue and methyl orange dyes. Applied Physics A 2022, 128.